Synthesis, Characterization and Water Oxidation Activity of Isomeric Ru-Complexes

Md Asmaul Hoque,[1] Abhishek Dutta Chowdhury,[3] Somnath Maji,[1] Jordi Benet-Buchholz,[1] Mehmed Z. Ertem,[2*] Carolina Gimbert-Suriñach,[1,4*] Goutam Kumar Lahiri,[3*] Antoni Llobet[1,4*]

[1] *Institute of Chemical Research of Catalonia (ICIQ), Av. Països Catalans 16, 43007 Tarragona,*

[2]*Chemistry Division, Energy & Photon Sciences Directorate, Brookhaven National Laboratory, Upton, New York 11973-5000, United States*

[3]*Department of Chemistry, Indian Institute of Technology Bombay, Powai, Mumbai 400076, India*

[4]*Universitat Autònoma de Barcelona, Departament de Química, Cerdanyola del Vallès, 08193 Barcelona, Spain*

Corresponding email: mzertem@bnl.gov., carolina.gimbert@uab.cat, lahiri@chem.iitb.ac.in, allobet@iciq.cat

Abstract

The synthesis and characterization of the isomeric ruthenium complexes with the general formula *cis*- and *trans*-[Ru(trpy)(qc)X]$^{n+}$ (trpy is 2,2':6',2''-terpyridine, qc is 8-quinolinecarboxylate, *cis*-**1** and *trans*-**1**, X = Cl, n = 0; *cis*-**2** and *trans*-**2**, X = OH_2, n = 1) with respect to the relative disposition of the carboxylate and X ligands is reported. For comparison purposes, another set of ruthenium complexes with general formula *cis*- and *trans*-[Ru(trpy)(pic)(OH_2)]$^{+}$ (pic is 2-picolinate (*cis*-**3**, *trans*-**3**) have been prepared. The complexes with qc ligand show a more distorted geometry as compared to the complexes with pic ligand. In all the cases, the *trans*-isomers show lower potential values for all the redox couples relative to the *cis*-isomers. Complexes *cis*-**2** and *trans*-**2** with six-member chelate ring show higher catalytic activity than *cis*-**3** and *trans*-**3**. Overall, it was shown that the electronic perturbation to the metal center exerted by different orientation and geometry of the ligands significantly influences both redox properties and in catalytic performance.

Keywords: Ruthenium, Isomers, Geometry, Redox properties, Water oxidation catalysis

1. Introduction

The conversion of solar energy to chemical energy is considered a promising option for the generation of renewable and clean fuels.[1] One way of achieving this goal is by performing light induced water splitting into hydrogen and oxygen as indicated in equation 1, catalyzed by suitable molecular catalysts,

$2H_2O_{(l)} + h\nu \rightarrow 2H_{2(g)} + O_{2(g)}$, $\Delta E^o = 1.23$ V *vs*. NHE.[2] (1)

In this process, the water oxidation half reaction is particularly challenging due to the large endothermicity and mechanistic complexity of the reaction that requires the transfer of four electrons and four protons with concomitant generation of an O-O bond.[3] For this reason, the study of new molecular water oxidation catalysts (WOC) has become one of the main research areas in the field, achieving tremendous progress in the last ten years. Among the most studied catalysts are those based on ruthenium, starting from the first well characterized blue dimer *cis*,*cis*-$[(bpy)_2(H_2O)Ru^{III}ORu^{III}(OH_2)(bpy)_2]^{4+}$, where bpy is 2,2'-bipyridine[4] to the recently reported fastest molecular WOC based on mononuclear Ru complexes $[Ru(bda)(isoq)_2]$,[5] $[Ru(tda)(py)_2]$,[6] $[Ru(pdc)(bpy)_2]$[7], $[Ru(mcbp)(py)_2]$[8] and $[Ru^{II}(H_3tPa\text{-}\kappa\text{-}N^3O)(py)_2]^+$,[9] ($bda^{2-}$ is (2,2'-bipyridine)-6,6'-dicarboxylate, tda^{2-} is 2,2':6',2''-terpyridine-6,6''-dicarboxylate, pdc^{2-} is pyridine-2,6-dicarboxylate, $mcbp^{2-}$ is 2,6-bis(1-methyl-4-(carboxylate)benzimidazol-2-yl)pyridine, H_3tPa is 2,2':6',2''-terpyridine-6,6''- diphosphonic acid, isoq is isoquinoline and py is pyridine). Further, these catalyst precursors have also been successfully used in water oxidation reactions triggered by light.[10,11,12,13,14]

The ability of Ru-OH_2 derivatives to undergo facile pH-dependent proton-coupled electron-transfer (PCET) processes is the key that leads to the formation of highly oxidized Ru^V=O species capable of O-O bond formation via water nucleophilic attack (WNA)[15,16,17] due to the electrophilicity of the Ru=O intermediate, dimerization through oxyl radical formation (I2M)[5,18] or oxygen atom transfer (OAT) via coupling of Ru–O and N–O moieties.[19,20] This significant information based on spectroscopic, electrochemical and analytical techniques together with the valuable complementary information provided by computational studies, has allowed a rational design for powerful and oxidatively rugged molecular water oxidation catalysts.[21,22,23,24,25]

The present report describes the synthesis, structural and spectroscopic characterization as well as the water oxidation catalytic activity of single site Ru-aquo isomeric complexes and their precursors with general formula *cis*- and *trans*-[Ru(trpy)(qc)Cl] (*cis*-**1,** *trans*-**1**) and *cis*- and *trans*-

[Ru(trpy)(qc)(OH_2)]$^+$ (*cis*-**2,** *trans*-**2**), where trpy is 2,2':6',2''-terpyridine and qc is 8-quinolinecarboxylate. In addition, two other similar complexes *cis*- and *trans*-[Ru(trpy)(pic)(OH_2)]$^+$ where pic is 2-picolinate (*cis*-**3**, *trans*-**3**) have also been studied for comparative purposes (Chart 1 and Scheme 1). The choice of qc and pic ligands is expected to provide information about how geometric isomers with different chelating ring sizes that can have the carboxylate group coordinated either in *cis* or *trans* fashion to the reactive Ru=O active species, can influence the performance of the water oxidation catalyst.

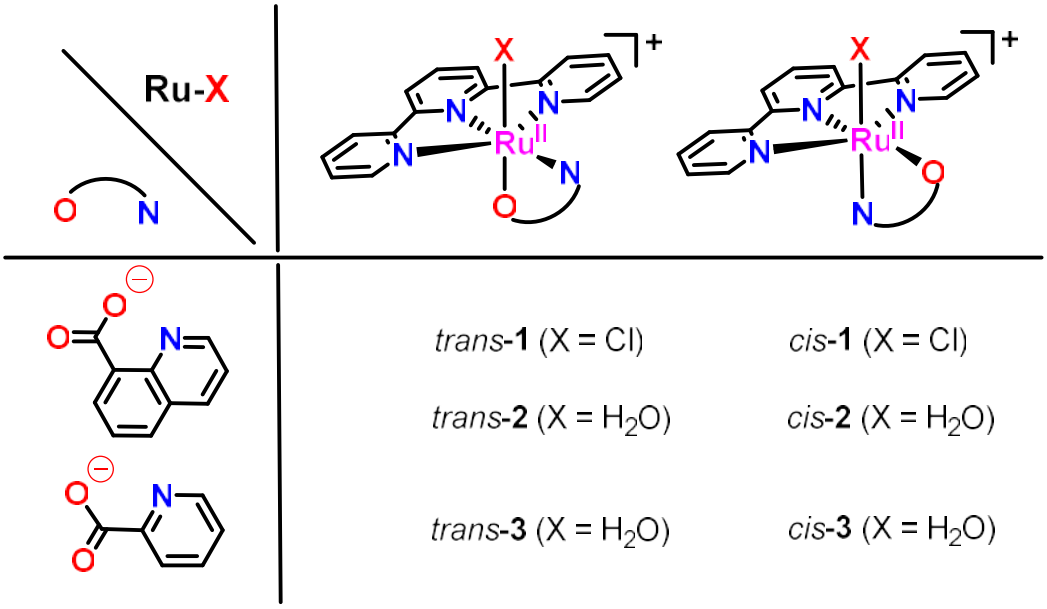

Chart 1. Ruthenium complexes studied in this work.

2. Experimental Section

Materials

The precursor complexes $[RuCl_3(trpy)]$ (trpy = 2,2':6',2''-terpyridine), *trans*-$[Ru^{II}(trpy)(pic)Cl]$, *cis*-$[Ru^{II}(trpy)(pic)Cl]$, *trans*-$[Ru^{II}(trpy)(pic)(OH_2)]ClO_4$ and *cis*-$[Ru^{II}(trpy)(pic)(OH_2)]ClO_4$ were prepared according to the literature procedures.[26,27] The ligand 8-quinolinecarboxylic acid and other reagents and chemicals were obtained from Aldrich and used as received. When required, solvents were dried by following the standard procedures, distilled under nitrogen and used immediately. High purity deionized water used for the electrochemistry experiments were obtained by passing distilled water through a nanopure Milli-Q water purification system. For other spectroscopic and electrochemical studies, HPLC-grade solvents were used.

Instrumentation and Methods

NMR spectra were recorded on a 500 MHz Bruker Avance Ultrashield NMR spectrometer. UV/Vis spectroscopy was performed on a Cary 50 (Varian) UV/Vis spectrophotometer in 1 cm quartz cuvettes. ESI-Mass spectra were recorded using micromass Q-TOF mass spectrometer. Elemental analyses were carried out on Perkin-Elmer 240C elemental analyzer. Cyclic voltammetry (CV), differential pulse voltammetry (DPV) experiments were performed on an IJ-Cambria CHI-660 potentiostat using a three-electrode cell. Typical CV experiments were carried out at a scan rate of 100 mVs^{-1}. The DPV parameters were ΔE = 4 mV, Amplitude = 50 mV, Pulse width = 0.05 s, Sampling width = 0.0167 s, Pulse period = 0.5 s. A glassy carbon disk (ϕ = 0.3 cm, S = 0.07 cm^2) was used as working electrode (WE), Pt disk as counter electrode (CE), and a Hg/Hg_2SO_4 (K_2SO_4 saturated) as a reference electrode (RE). All potentials were converted to NHE by adding 0.65 V. Glassy carbon electrodes were polished with 0.05 μm alumina (Al_2O_3) and rinsed with water and acetone followed by blow-drying before each measurement. CVs and DPVs were *i*R compensated by the potentiostat in all the measurements. In organic solvents, all the complexes were dissolved in CH_3CN containing the necessary amount of $[(n\text{-}Bu)_4N][PF_6]$ (TBAH) as supporting electrolyte to yield a 0.1 M ionic strength solution. In aqueous solutions, the electrochemical experiments were carried out in 0.1 M CF_3SO_3H (pH 1.0). $E_{1/2}$ values reported in this work were estimated from CV experiments as the average of the oxidative and reductive peak potentials $(E_{p,a} + E_{p,c})/2$ or taken as E (I_{max}) from DPV measurements. The Pourbaix diagrams were built using the following buffers: sodium dihydrogen phosphate/phosphoric acid up to pH 4 (pK_a = 2.12), sodium hydrogen phosphate/sodium dihydrogen phosphate up to pH 9 (pK_a = 7.67), sodium hydrogen phosphate/sodium phosphate up to pH 13 (pK_a = 12.12) and also 0.1 M CF_3SO_3H for pH 1.0. The concentration of the complexes was approximately 1 mM. The pH of

the solutions was determined by a pH meter (CRISON, Basic 20^{+}) calibrated before measurements through standard solutions at pH 4.01, 7.00 and 9.21.

Online manometric measurements were performed on a Testo 521 differential pressure manometer with an operating range of 0.1-10 kPa and accuracy within 0.5% of the measurements. The manometer was coupled to thermostatic reaction vessels for dynamic monitoring of the headspace pressure above each reaction solution. The manometer's secondary ports were connected to thermostatic reaction vessels containing the same solvents and headspace volumes as the sample vials. Each measurement for a reaction solution (2.0 mL) was performed at 298 K.

Single Crystal X-Ray Structure Determination

Crystal Preparation: Single crystals of *cis*-**1**, *trans*-**1**, *trans*-**2** and *cis*-[Ru^{II}(trpy)(pic)Cl] were grown by slow evaporations of 1:1 methanol:dichloromethane, 1:1 dichloromethane:diethylether, 1:1 dichloromethane: toluene and 1:1 methanol:dichloromethane, respectively. The crystals used for structure determination were selected employing a Zeiss stereomicroscope using polarized light and prepared under inert conditions immersed in perfluoropolyether as protecting oil for manipulation.

Data Collection: Crystal structure determination for sample *cis*-**1**, *trans*-**1** and *cis*-[Ru^{II}(trpy)(pic)Cl] were carried out using a Apex DUO Kappa 4-axis goniometer equipped with an APPEX 2 4K CCD area detector, a Microfocus Source E025 IuS using MoK$_\alpha$ radiation, Quazar MX multilayer Optics as monochromator and an Oxford Cryosystems low temperature device Cryostream 700 plus (T = −173 ˚C). Crystal structure determination for samples Full-sphere data collection was used with ω and φ scans. *Programs used:* Data collection APEX-2,[28] data reduction Bruker Saint[29] V/.60A and absorption correction SADABS.[30]

Crystal structure determination for sample *trans*-**2** was carried out at −123 ˚C using a Xcalibur Sapphire3 goniometer using MoK$_\alpha$ radiation. *Programs used:* Data collection and reduction with CrysAlisPro[31] V/.60A and absorption correction with Scale3 Abspack scaling algorithm.[32]

Structure Solution and Refinement: Crystal structure solution was achieved using the computer program SHELXT.[33] Visualization was performed with the program SHELXle.[34] Missing atoms were subsequently located from difference Fourier synthesis and added to the atom list. Least-squares refinement on F^2 using all measured intensities was carried out using the program SHELXL 2015.[35] All non-hydrogen atoms were refined including anisotropic displacement

parameters. *cis*-**1**: The asymmetric unit contains two different compounds of the metal complex sharing its position (ratio 90:10) and one and half water molecules disordered in four positions (ratio: 0.50:0.50:0.25:0.25). The metal complex is coordinated with 90 % ratio to a chloride anion and with 10 % to a methanolate. *trans*-**2**: The asymmetric unit contains one molecule of the complex coordinated to a water molecule, one additional water molecule and one PF_6^- anion. The PF_6^- anion is disordered in two orientations (ratio 91:9). *cis*-[Ru^{II}(trpy)(pic)Cl]: The asymmetric unit contains one molecule of the complex and 0.75 molecules of dichloromethane. The dichloromethane molecules are highly disordered in four orientations/positions.

Synthesis of Isomeric [Ru^{II}(trpy)(qc)Cl] (*trans*-1 and *cis*-1). In a 100 mL two neck round bottom flask, [$RuCl_3$(trpy)] (100 mg, 0.23 mmol), 8-quinolinecarboxylic acid (Hqc) (55 mg, 0.32 mmol) and NEt_3 (0.2 mL, 1.5 mmol) were dissolved in 20 mL of degassed ethanol. The mixture was heated to reflux for 6 h under nitrogen atmosphere. The mixture was then evaporated to dryness and the resulting dark solid was dissolved in the minimum volume of CH_2Cl_2 and purified by chromatography using a neutral alumina column. The blue-violet solution corresponding to the major isomer *trans*-**1** was eluted first with CH_2Cl_2:CH_3OH (20:1) followed by the red-violet solution of the minor isomer *cis*-**1** with CH_2Cl_2:CH_3OH (10:1) mixture. On removal of the solvent under reduced pressure the pure isomeric complexes *trans*-**1** and *cis*-**1** were obtained in the solid state.

***trans*-1:** Yield, 85 mg (0.16 mmol, 70%). Anal. Calcd. for ($C_{25}H_{17}N_4ClO_2Ru$): C, 55.35%; H, 3.16%; N, 10.33%. Found: C, 55.57%; H, 2.96%; N, 10.51%. λ [nm](ε[$M^{-1}cm^{-1}$]) in dicholoromethane: 578(11760), 420(10590), 328(38760), 315(34350), 281(38920), 233(74070). ESI^+-MS (*m/z*): 543.30 ([*trans*-**1**+H]$^+$, Calcd. 543.01), 507.30 ([*trans*-**1**-Cl]$^+$, Calcd. 507.03). ^{1}H NMR (500 MHz [d_6]-DMSO) δ: 10.43 (H^7, d, *J*= 4.86 Hz, 1H), 8.81 (H^9, d, *J*= 8.01 Hz, 1H), 8.63 ($H^{4\&5}$, dd, *J*= 7.7 Hz and *J*=2.83 Hz, 4H), 8.51 (H^{12}, d, *J*= 7.45Hz, 1H), 8.40 (H^{10}, d, *J*= 7.82, 1H), 8.0 (H^1, d, *J*= 5.47 Hz, 2H), 7.92 ($H^{3,6\&8}$, m, 4H), 7.77 (H^{11}, t, *J*= 7.7 Hz, 1H), 7.41 (H^2, t, *J*= 6.5 Hz, 2H). ^{13}C-NMR (125 MHz, [d_6]-DMSO) δ: 169.1, 160.6, 160.4, 158.5, 152.2, 147.8, 138.2, 136.7, 136.2, 133.7, 131.3, 130.6, 130.5, 127.2, 127.0, 123.2, 121.9 and 121.5.

***cis*-1:** Yield, 6 mg (0.01 mmol, 4%). Anal. Calcd. for ($C_{25}H_{17}N_4ClO_2Ru$): C, 55.35%; H, 3.16%; N, 10.33%. Found: C, 55.27%; H, 3.10%; N, 10.58%. λ [nm](ε[$M^{-1}cm^{-1}$]) in acetonitrile: 545(11360), 483(sh), 372(11300), 317(46680), 279(42080), 235(79690). ESI^+-MS (*m/z*): 543.19 ([*cis*-**1**+H]$^+$, Calcd. 543.01), 507.10 ([*cis*-**1**-Cl]$^+$, Calcd. 507.03). ^{1}H NMR (500MHz [d_6]-DMSO) δ: 9.0 (H^7, dd, *J*= 4.86 Hz, and *J*= 1.7 Hz, 1H), 8.62 ($H^{1,4\&5}$, m, 6H), 8.06 (H^{10} dd, *J*= 8.31 Hz and *J*= 1.31 Hz, 1H), 7.95 ($H^{2\&9}$, m, 3H), 7.82 (H^6, t, *J*=7.98, 1H), 7.73 (H^8, t, *J*= 7.74 Hz, 1H), 7.56 (H^3, dt, *J*= 5.65 Hz and *J*= 1.14 Hz, 2H), 7.05 (H^{12}, dd, *J*= 5.41 and Hz *J*= 1.43 Hz, 1H), 6.82 (H^{11}, dd, *J*= 8.16 Hz and *J*= 5.45

Hz, 1H). ^{13}C-NMR (125MHz, [d_6]-DMSO) δ: 169.1, 161.4, 159.7, 153.7, 151.5, 148.2, 137.4, 136.7, 136.4, 133.3, 131.6, 129.3, 129.1, 127.6, 127.1, 123.4, 122.5 and 121.3.

Synthesis of *trans*-[Ru^{II}(trpy)(qc)(OH$_2$)](PF$_6$) (*trans*-2). In a 50 mL two neck round bottom flask, *trans*-**1** (100 mg, 0.18 mmol) was dissolved in 20 mL of acetone: water mixture (3:1, *v/v*) and $TlNO_3$ (60 mg, 0.23 mmol) was added to the solution and stirred for 1 h at reflux. The initial blue-violet color of the solution changed to red-violet with the precipitation of TlCl. The cooled solution was filtered over Celite® to remove TlCl. The filtrate was then concentrated to approx. 2 mL in vacuum and 3 mL saturated solution of NH_4PF_6 was added. The resulting solution was allowed to stand at 0˚C for complete precipitation. It was then filtered and the product was washed with ice-cold water for several times and dried in vacuum over P_4O_{10}. Yield: 110 mg (0.16 mmol, 88%). Anal. Calcd. for ($C_{25}H_{19}N_4O_3RuPF_6$): C, 44.78%; H, 2.86%; N, 8.36%. Found: C, 44.98%; H, 2.95%; N, 8.62%. ESI$^+$-MS (*m/z*): 507.10 ({*trans*-**2**-PF$_6$-OH$_2$}$^+$, Calcd. 507.03). ^{1}H NMR (500MHz, [d_2]-D_2O) δ: 9.59 (H^7, d, *J*= 5.52 Hz, 1H), 8.73 (H^9, d, *J*= 8.41 Hz, 1H), 8.39 (H$^{4,5,10\&12}$, m, 6H), 8.08 (H^1, d, *J*= 5.60Hz, 2H), 7.89 (H$^{3,8\&11}$, m, 4H), 7.77 (H^6, t, *J*= 7.65 Hz, 1H), 7.31 (H^2, t, *J*= 6.93 Hz, 2H). ^{13}C- NMR (125MHz, [d_2]-D_2O) δ: 175.2, 160.7, 160.3, 155.3, 153.2, 147.6, 138.8, 137.5, 137.2, 135.4, 134.0, 130.7, 127.1, 127.0, 123.4, 123.2, 122.1 and 121.8.

Synthesis of *cis*-[Ru^{II}(trpy)(qc)(OH$_2$)]$^+$ (*cis*-2). In a 25 mL two neck round bottom flask, *cis*-**1** (5 mg, 0.01 mmol) was dissolved and $TlNO_3$ (5 mg, 0.02 mmol) was suspended in 4 mL of acetone:water mixture (3:1, *v/v*) and stirred for 1 h at reflux. The initial red-violet color of the solution was changed to red with the precipitation of TlCl. The cooled solution was filtered to remove TlCl. The filtrate was dried in vacuum over P_4O_{10} and dissolved in D_2O for NMR and pH 1 for electrochemistry. ^{1}H NMR (500MHz, [d_2]-D_2O) δ: 8.97 (H^7, d, *J*= 7.63 Hz, 1H), 8.56 (H^1, d, *J*= 5.48 Hz, 2H), 8.37 (H^5, d, *J*= 8.25 Hz, 2H), 8.31 (H^4, d, *J*= 8.11 Hz, 2H), 7.98 (H^9, d, *J*= 8.09 Hz, 1H), 7.88 (H$^{3,6\&10}$, m, 4H), 7.72 (H^8, t, *J*= 7.96 Hz, 1H), 7.40 (H^2, t, *J*= 6.65 Hz, 2H), 7.30 (H^{12}, d, *J*= 5.37 Hz, 1H), 6.62 (H^{11}, dd, *J*= 7.95 Hz and *J*= 5.93 Hz, 1H).

Computational Methods

Geometry optimizations were performed at the M06[36] level of density functional theory coupled with SMD aqueous continuum solvation model[37] using the Stuttgart [8s7p6d2f | 6s5p3d2f] ECP28MWB contracted pseudopotential basis set[38] on Ru and the 6-31G(d) basis set[39] on all other atoms. Non-analytical integral evaluations made use of a pruned grid having 99 radial shells and 590 angular points per shell as implemented in Gaussian 16 software package.[40] The nature of all stationary points was verified by analytic computation of vibrational frequencies, which were also used for the computation of zero-point vibrational energies and molecular

partition functions. Partition functions were used in the computation of 298 K thermal contributions to free energy employing the usual ideal-gas, rigid-rotator, harmonic oscillator approximation.[41] Free energy contributions were added to single-point M06-L[42], MN15-L[43], B3LYP-D3[44,45], ωB97X-D[46], M06 and MN15[47] electronic energies computed with SMD aqueous continuum solvation model and the SDD basis set on ruthenium and the 6-311+G(2df,p) basis set on all other atoms to arrive at final composite free energies.

A 1 M standard state was used for all species in aqueous solution except for water itself, for which a 55.6 M standard state was employed. Thus, for all molecules but water, the free energy in aqueous solution is computed as the 1 atm gas-phase free energy, plus an adjustment for the 1 atm to 1 M standard-state concentration change of *RT* ln (24.5), or 1.9 kcal/mol, plus the 1 M to 1 M transfer (solvation) free energy computed from the SMD model. In the case of water, the 1 atm gas-phase free energy is adjusted by the sum of a 1 atm to 55.6 M standard-state concentration change, or 4.3 kcal/mol, and the experimental 1 M to 1 M solvation free energy, –6.3 kcal/mol. The 1 M to 1 M solvation free energy of the proton was taken from experiment as –265.9 kcal/mol.[48,49,50,51]

Standard reduction potentials were calculated for various possible redox couples. For a redox reaction of the form

$$O_{(\mathrm{aq})} + n\, e^-_{(\mathrm{g})} \rightarrow R_{(\mathrm{aq})} \qquad (2)$$

where *O* and *R* denote the oxidized and reduced states of the redox couple, respectively, and *n* is the number of electrons involved in redox reaction, the reduction potential $E^0_{O/R}$ relative to NHE was computed as

$$E^{\mathrm{o}}_{O|R} = -\frac{\Delta G^{\mathrm{o}}_{O|R} - \Delta G^{\mathrm{o}}_{\mathrm{NHE}}}{nF} \qquad (3)$$

where $\Delta G^0_{O/R}$ is the free energy change associated with equation 2 (using Boltzmann statistics for the electron), ΔG^0_{NHE} is the free energy change associated with

$$\mathrm{H}^+_{(\mathrm{aq})} + e^-_{(\mathrm{g})} \rightarrow \frac{1}{2}\mathrm{H}_{2(\mathrm{g})} \qquad (4)$$

which is –4.28 eV with Boltzmann statistics for the electron,[52,53] and *F* is the Faraday constant.

3. Results and Discussion

3. 1. Synthesis, Spectroscopy and Structural Characterization

The synthetic strategy used for the preparation of the complexes described in this work is outlined in Scheme 1. The reaction of 8-quinolinecarboxylic acid with the ruthenium precursor complex $[RuCl_3(trpy)]$ in the presence of NEt_3 in EtOH results in a 15:1 mixture of isomeric complexes of *trans*- and *cis*-$[Ru^{II}(trpy)(qc)Cl]$ (*trans*-**1** and *cis*-**1**) respectively**.** The *cis* and *trans* assignment refers to the relative disposition of the chlorido and carboxylato ligands. Both isomers can be separated by column chromatography and are stable in the solid state and in solution. The corresponding *trans*- and *cis*-isomeric aquo complexes $[Ru(trpy)(qc)(OH_2)]^+$ (*trans*-**2** and *cis*-**2**) have been synthesized *via* substitution of the chlorido ligand by H_2O using $TlNO_3$ in acetone:H_2O (3:1) as the solvent mixture and formation of insoluble TlCl. Complexes *trans*-**1**, *cis*-**1**, *trans*-**2** and *cis*-**2** have been thoroughly characterized by means of analytical, spectroscopic and electrochemical techniques.

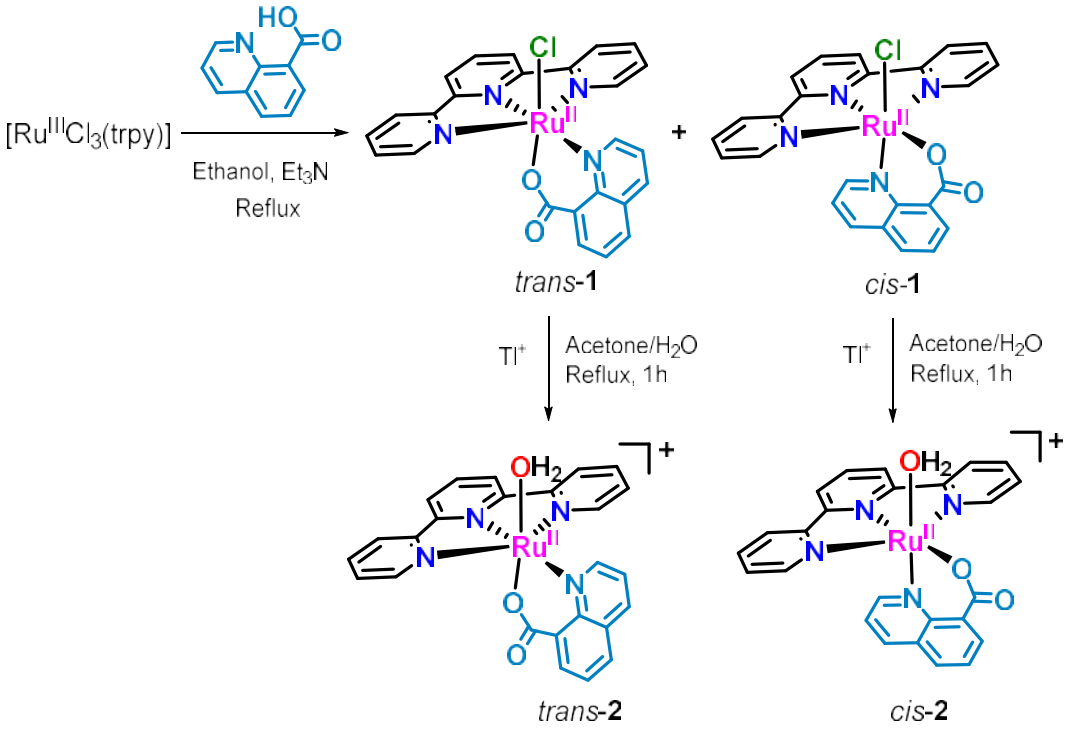

Scheme 1. Synthetic strategy and labelling scheme used for the complexes described in this work.

Single crystals of the complexes *trans*-**1**, *cis*-**1** and *trans*-**2** together with the related picolinate derivative *cis*-[Ru(trpy)(pic)Cl] were obtained and their ORTEP structures are shown in Figure 1. All the complexes display the typical slightly distorted octahedral geometry around the ruthenium, as expected for low-spin d^6 Ru^{II}.[54,55] The bidentate ligand 8-quinolinecarboxylate occupies both axial and equatorial positions and is bonded to the ruthenium metal *via* the anionic oxygen atom O1 (carboxylate) and neutral nitrogen atom N1 (quinoline) (see Figure 1 for the labeling key) donors forming a six-membered chelate ring. The meridional configuration of trpy introduces expected geometrical constraint as has been reflected in NRuN *trans* angle involving the trpy ligand (for *trans*-**1**, the N2-Ru-N4 angle is 160.21(17); for *trans*-**2**, the N2-Ru-N4 angle is 159.26(13)). The central Ru-N3(trpy) bond length is 1.955(4) Å and 1.942(4) Å in *trans*-**1** and *trans*-**2**, respectively, which is significantly shorter than the corresponding distances involving the terminal pyridine rings of trpy (for *trans*-**1**, Ru-N2(trpy) is 2.061(5) Å and Ru-N4(trpy) is 2.058(5); for *trans*-**2** these values are 2.064(4) and 2.058(3) Å respectively). On other hand, the Ru-N1(qc) in *trans* to the Ru-N3(trpy) bonds are slightly longer, 2.129(4) and 2.085(3) Å.[56] The Ru-O3(H_2O) bond distance of 2.094(3) Å in *trans*-**2** agrees well with the reported analogous ruthenium-aquo species.[57]

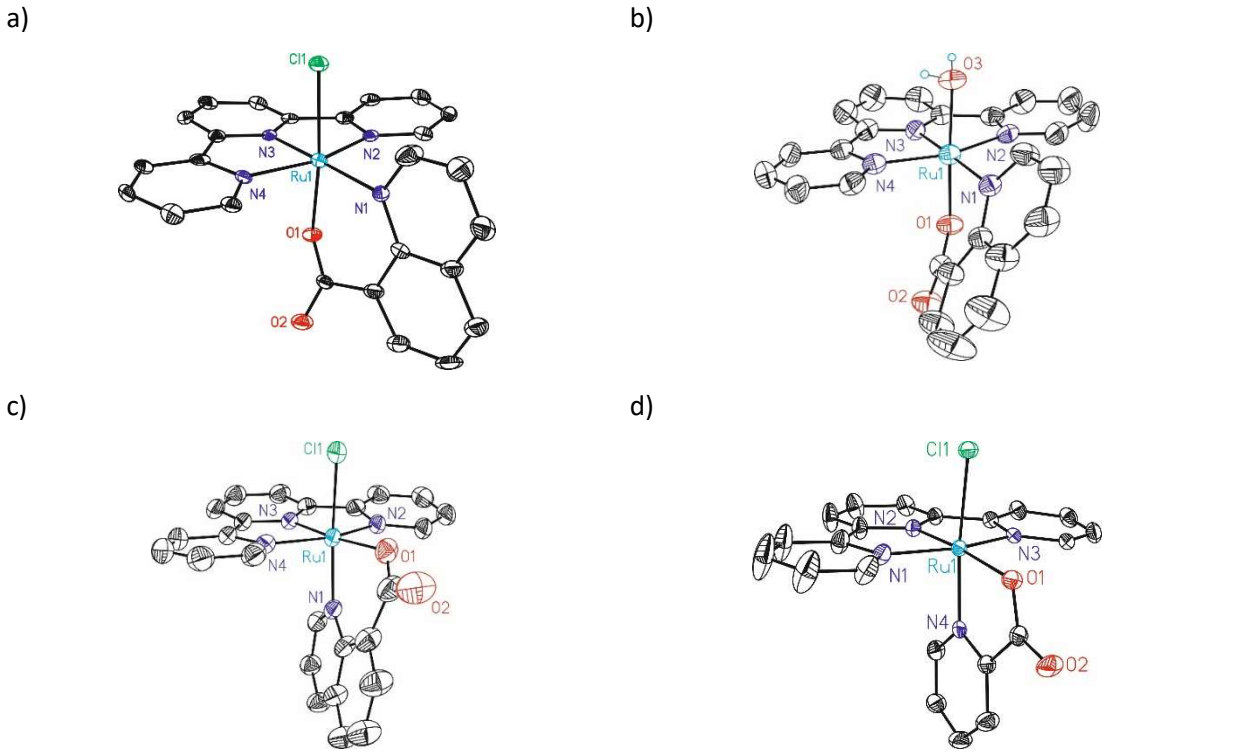

Figure 1. ORTEP diagrams of (a) *trans*-[Ru(trpy)(qc)Cl] (*trans*-**1**), (b) *trans*-[Ru(trpy)(qc)$(OH_2)]^+$ (*trans*-**2**), (c) *cis*-[Ru(trpy)(qc)Cl] (*cis*-**1**) and (d) *cis*-[Ru(trpy)(pic)Cl]. Thermal ellipsoids are drawn at 50% probability. The solvents of crystallization and hydrogen atoms are omitted for clarity, except for the OH_2 ligand.

The Ru-Cl bond distance in *trans*-**1** (2.4197(13) Å) is 0.03 Å longer than that in *cis*-**1** (2.393(12) Å).[58] We attribute this difference to the electronegativity of the Cl ligand and to the presence of strong σ–donating negatively charge O^- of qc trans to Cl^- in *trans*-**1** as compared to *cis*-**1**, where the neutral N of the qc is trans to Cl^-. This in turn makes the Ru-O bond shorter in *trans*-**1** (2.049(3) Å) relative to *cis*-**1** (2.085(3) Å). On the other hand, the Ru-N1(qc) distance in *cis*-**1** (2.061(3) Å) is shorter than that in *trans*-**1** (2.129(4) Å), mainly due to the enhanced $Ru^{II}\rightarrow$quinoline back-bonding via involvement of σ- and π-donating chlorido ligand trans to N1(qc) in *cis*-**1**. They also show appreciable differences in the trans angle involving qc-Ru-Cl: O1-Ru-Cl at 174.21(11)˚ in *trans*-**1** vs N1-Ru-Cl at 172.93(10)˚ in *cis*-**1**; the bulkier quinoline ring trans to Ru-Cl in *cis*-**1** makes it relatively bent (Figure S12 and Tables S2-S3). Interestingly, the dihedral angles between the planes of qc and trpy in *cis*-**1**, qc-Ru-trpy, is 76.2˚ and for the analog complex having the picolinate ligand *cis*-[Ru(trpy)(pic)Cl], the angle pic-Ru-trpy is 87.6˚ (Figure S13). This difference clearly indicates the presence of more distortion in the complex containing the qc ligand as compared to that of the complex containing the pic ligand. The computed structural parameters at M06 level of theory are overall in good agreement with X-ray crystal structures and corroborates the experimental observations such as the distortion in the *cis*-**1** complex (Table S2). One important distinction is that the *trans* effect is much less pronounced in computed structures and especially nonexistent for the Ru-Cl bond distances of *trans*-**1** and *cis*-**1**.

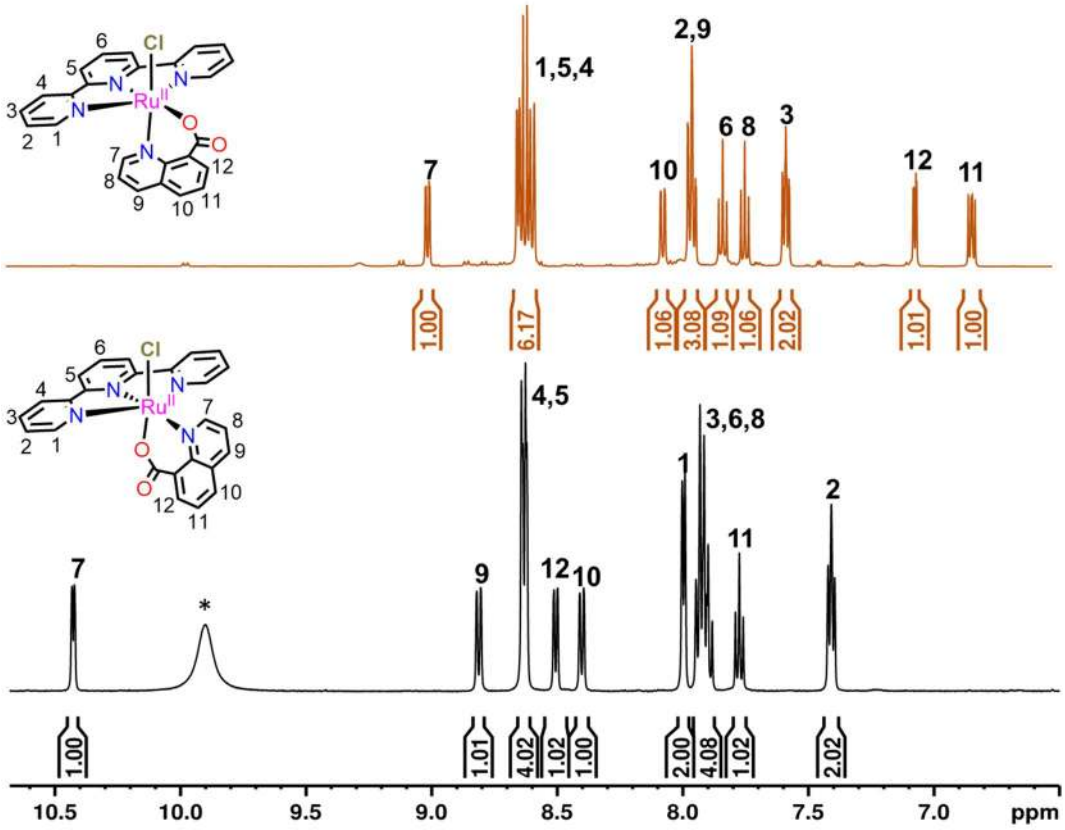

Figure 2. ^{1}H NMR spectra in [d_6]-DMSO (500 MHz, 298 K) and corresponding assignment for complexes *cis*-**1** (top) and *trans*-**1** (bottom). Asterisk indicates unidentified species.

The ^{1}H NMR spectra of *trans*-**1** and *cis*-**1** are quite distinct, as expected (Figure 2). In both cases, the symmetric nature of the complexes observed in the solid state is maintained in solution as indicated by a single set of signals for the trpy ligand. A characteristic feature of *trans*-**1** is the typical signal at low field δ = 10.4 ppm[59] for a proton in *ortho* to the quinoline nitrogen of the bidentate ligand (proton H^7) de-shielded due to the diamagnetic anisotropy generated by the chlorido ligand,[60,61] allowing us to fully assign all the signals. A further clue in this direction is given by the NOE signal between H^7 and H^1 (with a distance of 2.72 Å in the solid-state structure, see Figure S1-S3). None of these features are present in the spectrum of *cis*-**1**, so its assignment is based on intensities of the integrals with the help of 2-dimensional experiments (Figure S4-S6). The NMR analysis of complexes *trans*-**2** and *cis*-**2** were performed in deuterated water to avoid ligand exchange with coordinating ligands such as DMSO. Compound *trans*-**2** also shows the typical downfield signal of H7 due to anisotropic effects with the aquo ligand (δ = 9.6 ppm, Figure S7 and S11).

3. 2. Electrochemical Characterization

The redox properties of all the complexes were analyzed by cyclic voltammetry (CV) and differential pulse voltammetry (DPV) in acetonitrile (CH_3CN) containing 0.1 M of [(*n*-Bu)$_4$N][PF_6] (TBAH) for complexes *trans*-**1** and *cis*-**1** and 0.1 M ionic strength buffered aqueous solutions at different pHs for complexes *trans*-**2** and *cis*-**2**. All redox potentials reported in this work were measured with Hg/Hg_2SO_4 reference electrode and referred to the NHE electrode.

In acetonitrile solution, both *trans*-**1** and *cis*-**1** isomers show a chemically reversible and electrochemically quasi-reversible one-electron oxidation wave at $E_{1/2}$ = 0.58 V (ΔE = 60 mV) and $E_{1/2}$ = 0.67 V (ΔE = 63 mV) respectively, assigned to the $Ru^{III/II}$ redox couple (Figure S14). The slight cathodic shift of the $Ru^{III/II}$ couple observed for *trans*-**1** as compared to *cis*-**1** is attributed to the higher electron density on the ruthenium provided by the chlorido and carboxylato moieties when they are in *trans* relative position. This trend agrees with the shorter Ru-O and Ru-Cl distances observed in the solid-state structure of *trans*-**1** as compared to *cis*-**1** and highlights the strong influence of the relative position (*trans vs. cis*) of the ligands.

The redox chemistry of the aquo complexes *trans*-**2** and *cis*-**2** were studied in pH 1 (0.1 M triflic acid) solution and the appropriate phosphate buffer for measurements at pH > 1 (Figure S16). Both isomers exhibit two successive pH dependent redox couples associated with proton-coupled electron-transfer (PCET) processes with the formation of the Ru^{III} and Ru^{IV} species with different level of protonation of the aquo group, hydroxo or aquo depending on the pH (Equations 5 and 6). Further scanning to more positive potentials shows a third pH independent oxidation leading to the [Ru^{V}=O] (Equation 7) which is followed by a large anodic current attributed to the electrocatalytic oxidation of water to produce oxygen gas (Figure 3a).

$$[Ru^{II}(trpy)(qc)(H_2O)]^{+}_{(aq)} \rightarrow [Ru^{III}(trpy)(qc)(OH)]^{+}_{(aq)} + H^{+}_{(aq)} + e^{-} \quad (5)$$

$$[Ru^{III}(trpy)(qc)(OH)]^{+}_{(aq)} \rightarrow [Ru^{IV}(trpy)(qc)(O)]^{+}_{(aq)} + H^{+}_{(aq)} + e^{-} \quad (6)$$

$$[Ru^{IV}(trpy)(qc)(O)]^{+}_{(aq)} \rightarrow [Ru^{V}(trpy)(qc)(O)]^{2+}_{(aq)} + e^{-} \quad (7)$$

Interestingly, the $[Ru^{III}\text{-}OH_2]^{2+}/[Ru^{II}\text{-}OH_2]^{+}$ redox couple for *trans*-**2** in pH 1 (0.67 V), is 150 mV lower as compared to *cis*-**2** (0.82 V), and this is due to the *trans* influence of the carboxylate group to the aquo ligand making the metal center electronically richer, hence easier to oxidize in good agreement with the computed values of 0.59 V and 0.69 V at MN15 level of theory for *trans*-**2** and *cis*-**2** respectively. On the other hand $[Ru^{V}\text{-}O]^{2+}/[Ru^{IV}\text{-}O]^{+}$ redox couple is only 90 mV lower (Table 1).

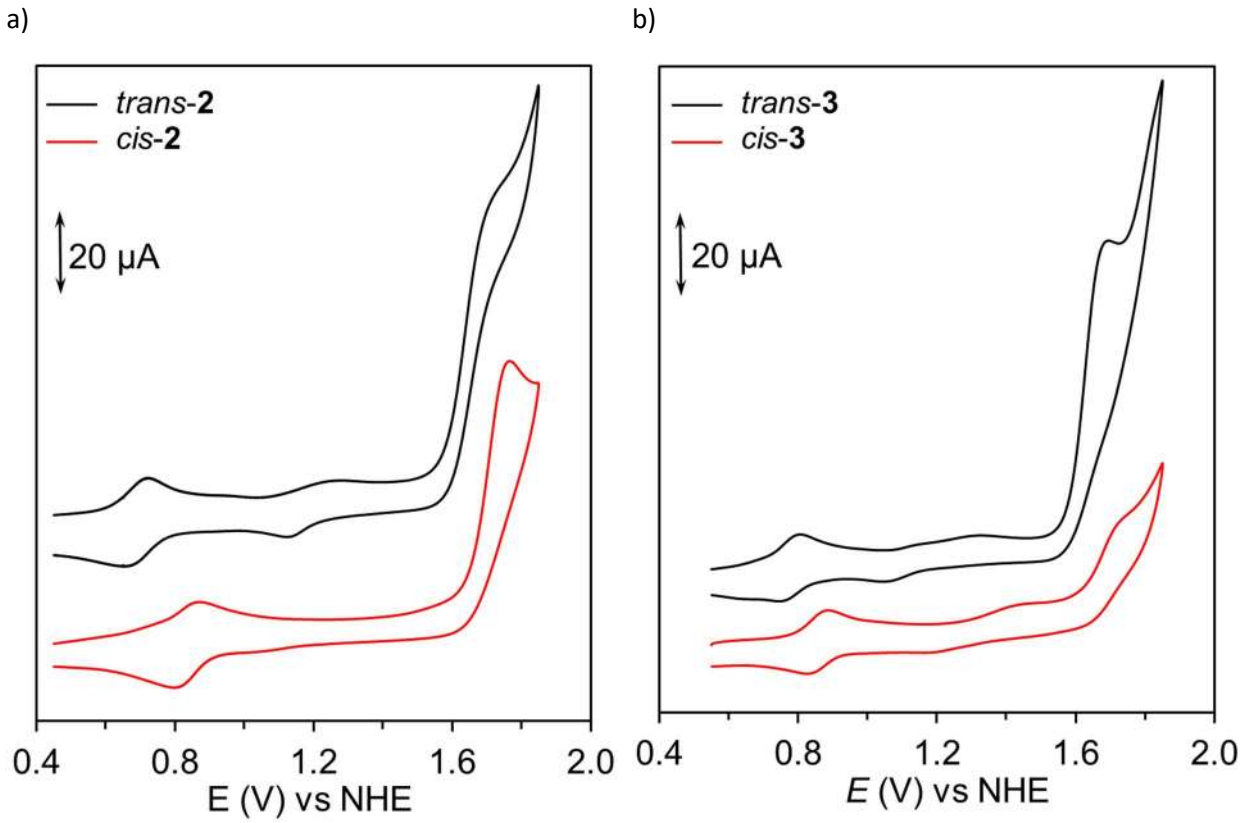

Figure 3. a) CVs of *trans*-**2** (black) and *cis*-**2** (red) in 0.1 M triflic acid (pH 1), b) CVs of *trans*-**3** (black) and *cis*-**3** (red) in 0.1 M triflic acid (pH 1). Working electrode: glassy carbon disk; counter electrode: platinum disk; reference electrode: Hg/Hg_2SO_4.

The Pourbaix diagrams for *trans*-**2** and *cis*-**2** (Figure 4) reveal that the $[Ru^{III}\text{-}OH]^{+}/[Ru^{II}\text{-}OH_2]^{+}$ and $[Ru^{IV}\text{-}O]^{+}/[Ru^{III}\text{-}OH]^{+}$ redox processes each changes by approximately 59 mV per pH decade over a large pH range (10 > pH > 2) for *trans*-**2** and (10 > pH > 3) for *cis*-**2**, respectively. The $Ru^{III/II}$ redox processes of *trans*-**2** (at pH < 2) and *cis*-**2** (at pH < 3) are not associated with the loss of a proton based on the pH-independent behavior of the $[Ru^{III}\text{-}OH_2]^{2+}/[Ru^{II}\text{-}OH_2]^{+}$ redox couple. Consequently, the higher oxidation step is accompanied with the loss of two protons (*i.e.* $[Ru^{IV}\text{-}O]^{+}/[Ru^{III}\text{-}OH_2]^{2+}$) in strongly acidic medium. This assignment is corroborated by the slope of −120 mV/pH below pH 2.0 for *trans*-**2** and −121 mV/pH below pH 3.0 for *cis*-**2**. At pH >10, the potentials for the $Ru^{IV/III}$ couple continue to vary linearly with pH, with a

slope near to –59 mV/pH unit, while the potentials for the $Ru^{III/II}$ couple become pH independent as a consequence of no loss of proton from $[Ru^{II}\text{-}OH]$ with pK_a ≈ 10.6. The $[Ru^{V}\text{-}O]^{2+}/[Ru^{IV}\text{-}O]^{+}$ redox couple remains relatively constant at ~1.62 V and ~1.71 V vs NHE for *trans*-**2** and *cis*-**2** respectively, over the whole pH 1-13 range.

It is worth mentioning that *cis*-**2** over time in aqueous solution slowly converts to *trans*-**2** as can be seen in Figure S16b and Figure S18. This is in good agreement with lower isolated yield of the *cis*-**1** compared to the *trans*-**1** indicating that the latter is thermodynamically more stable.

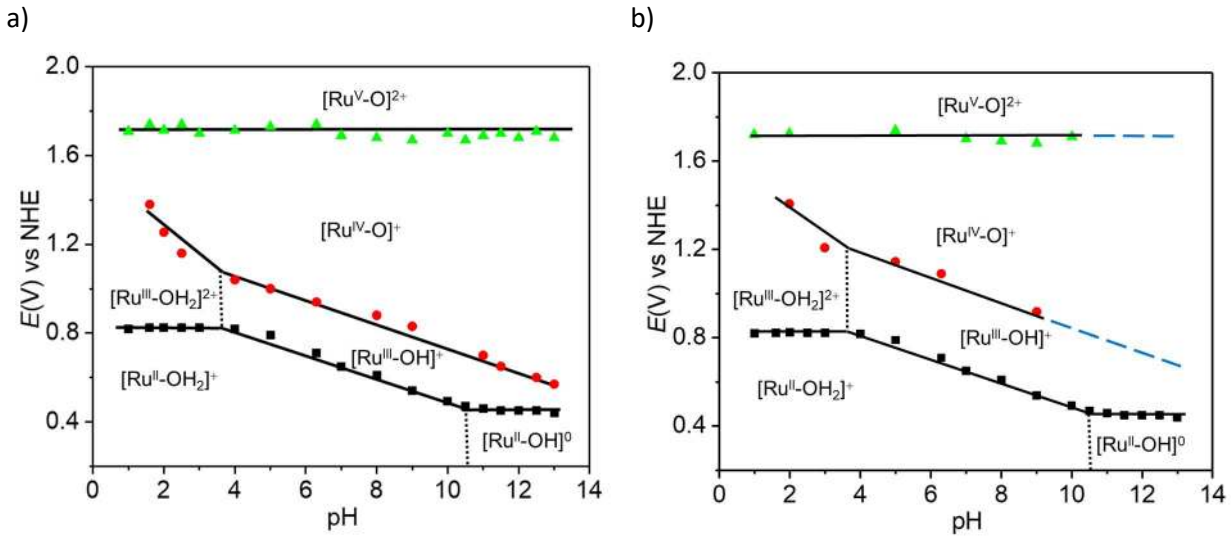

Figure 4. Pourbaix diagram of a) *trans*-$[(trpy)(qc)Ru^{II}(OH_2)]^+$, *trans*-**2** and b) *cis*-$[(trpy)(qc)Ru^{II}(OH_2)]^+$, *cis*-**2**. The black solid lines indicate the redox potentials for the different redox couples, whereas the dashed vertical lines indicate the p*K*a. The zone of stability of the different species are indicated only with the Ru symbol, its oxidation state, and the degree of protonation of the aquo ligand. For instance, "Ru^{V}-O" is used to indicate the zone of stability of *trans*-$[(trpy)(qc)Ru^{V}(O)]^{2+}$ for the *trans*-**1** (left) and *cis*-$[(trpy)(qc)Ru^{V}(O)]^{2+}$ for the *cis*-**2** (right). Blue dotted line corresponds to the imaginary line and extended of the corresponding redox potential.

In order to gain more insight into the *trans vs. cis* influence on the redox potentials and catalytic activity, we have extended our study to two similar mononuclear Ru-trpy-OH_2 complexes containing the 2-picolinate (pic) bidentate ligand, namely, *trans*-**3** and *cis*-**3** in Chart 1. These two complexes are of interest because they form a five-membered chelate ring around the metal center as opposed to the 8-quinolinecarboxylate (qc) which makes six-membered chelate rings, allowing us to further study the geometric effects. Complexes *trans*-**3** and *cis*-**3** have been synthesized and characterized according to the literature procedure[25] and here we have extensively studied their electrochemical and water oxidation properties.

As shown in the CVs in Figure 3b and the Pourbaix diagrams in Figure S17, complexes *trans*-**3** and *cis*-**3** also show two successive pH dependent redox couples associated with PCET processes and a third pH independent oxidation couple related to electrochemical oxidation of water to dioxygen. The redox potentials for the four Ru-aquo complexes in Chart 1 are summarized in Table 1 together with other relevant Ru-aquo complexes previously described in the literature.

An interesting feature arising from the comparison of the potentials is that at pH 1.0 the $Ru^{III/II}$ redox couple for *trans*-**2** is around 90 mV lower compared to the related *trans*-Ru(trpy)(pic) complex, *trans*-**3**. Considering that both complexes have a similar trans influence of the carboxylate group, we attribute this phenomenon to the higher distortion of the dihedral plane between the quinolinate and trpy ligands in *trans*-**2** as compared to that of the picolinate and trpy ligands in *trans*-**3** (Figure S13). The inspection of the optimized structures of $[Ru^{II}\text{-}OH_2]^{+}$ and $[Ru^{III}\text{-}OH_2]^{2+}$ shows that the Ru-O1 (carboxylate O) distance is shorter in *trans*-**2** compared to *trans*-**3** (2.04 vs 2.07 Å) for $[Ru^{II}\text{-}OH_2]^{+}$ and more importantly becomes even shorter (1.95 vs 2.00 Å) upon oxidation to generate $[Ru^{III}\text{-}OH_2]^{2+}$. This indicates that six-membered chelate ring of qc coupled with distortion of the dihedral plane between the qc and trpy ligands enables further stabilization of the $[Ru^{III}\text{-}OH_2]^{2+}$ species upon oxidation for *trans*-**2** compared to *trans*-**3**. On the other hand, for the $Ru^{III/II}$ redox couple *cis*-**2** is only 40 mV lower than *cis*-**3**. In contrast to *trans* isomers, although the Ru-O1 distance is shorter for *cis*-**2** and *cis*-**3** exhibits shorter Ru-N1 bond length which imparts a balancing effect. Therefore, this small difference is associated solely to changes in the geometry between the two complexes. Indeed, as shown in Figures S13, dihedral angles between the qc-trpy and pic-trpy planes in *cis*-**1** and *cis*-$[Ru^{II}$(trpy)(pic)Cl] are significantly different (76.2° and 87.6°, respectively).

In contrast, the third oxidation $[Ru^{V}{=}O]^{2+}/[Ru^{IV}{=}O]^{+}$ for *trans*-**2** is around 20 mV higher compared to the related *trans*-**3** and the same trend is observed for *cis*-**2**, which shows an anodic shift of 40 mV higher compared to *cis*-**3**. However, *trans* effect is observed for both complexes **2** (1.62 V vs 1.71 V) and **3** (1.60 V vs 1.67 V) for the $[Ru^{V}{=}O]^{2+}/[Ru^{IV}{=}O]^{+}$ redox couple.

The pK_a values for the $[Ru^{II}\text{-}OH_2]^{+}$ species do not differ significantly between two isomers whereas for the for $[Ru^{III}\text{-}OH_2]^{2+}$ species, the *cis*-isomers exhibit pK_a values slightly higher than the corresponding *trans*-isomers (compare entry 2 with 3 and entry 4 with 5 in Table 1 and Figure 4). On the other hand, the pK_a values of all these complexes with singly negatively charged carboxylate ligand are higher, compared to other Ru-aquo complexes with neutral ligand such as $[Ru(trpy)(bpy)(OH_2)]^{2+}$ as expected[62] (entry 1, Table 1) and similar to that of $[Ru(bpc)(bpy)(H_2O)]^{+}$ which also contains a carboxylate ligand (entry 7, Table 1, bpc = 2,2'-bipyridine-6-carboxylate).

Table 1. Thermodynamic and catalytic data for Ru-aqua carboxylate and related complexes described in the literature at pH 1.

		$E_{1/2}$ (V) *vs.* NHE				pK_a				
Entry	Complexes[a]	V/IV	IV/III	III/II	[b]ΔE (mV)	Ru^{II}-OH_2	Ru^{III}-OH_2	TON[c]	TOF[d]	TOF_{max}[e]
1[62]	$[Ru(trpy)(bpy)(H_2O)]^{2+}$	1.92	1.22	1.06	110	9.7	1.7	18.3	0.01	-
2[f]	*cis*-**2**	1.71(1.69)	-(1.23)	0.82(0.69)	-(540)	10.6	3.8	-		6.8
3[f]	*trans*-**2**	1.62(1.58)	1.20(1.06)	0.67(0.59)	530(470)	10.6	2.7	14.9	0.68	4.2
4[27,f]	*cis*-**3**	1.67(1.62)	1.31(1.27)	0.86(0.65)	450(620)	10.1	3.7	8.6	0.11	0.3
5[27,f]	*trans*-**3**	1.60(1.56)	1.09(0.94)	0.76(0.69)	330(250)	10.1	2.0	19.7	0.24	1.2
6[63]	$[Ru(pdc)(bpy)(H_2O)]^{+}$	1.41	1.19	0.52	670	11	4	-		0.2
7[64]	$[Ru(bpc)(bpy)(H_2O)]^{+}$	1.57	1.29	0.81	480	10.6	2.6	-	0.16	-

[a]Ligand abbreviations: trpy = 2,2′:6′,2″-terpyridine, bpy = 2,2′-bipyridine, pic = 2-picolinate, qc = 8-quinolinecarboxylate, bpc = 2,2′-bipyridine-6-carboxylate, pdc = 2,6-pyridinedicarboxylate. [b]ΔE= $E_{1/2}$(IV/III)-$E_{1/2}$(III/II); [c]TON stands for Turn Over Numbers; [d]TOF stands for initial Turn Over Frequency in s^{-1}; These values are extracted for the catalytic reactions involving 1.0 mM Cat/100 mM Ce^{IV} in a 0.1 M triflic acid solution with a total volume of 2 mL; [e]TOF_{max} stands for Maximum Turn Over Frequency reported in s^{-1}; values extracted from Foot of the Wave Analysis of CV and DPV experiment in pH 1 (entry 2-6); [f] this work; Redox potential values and pK_as in parenthesis are calculated from at MN15 level of theory.

We performed density functional theory (DFT) calculations to compute redox potentials for the $Ru^{III/II}$, $Ru^{IV/III}$ and $Ru^{V/IV}$ couples as well as pK_as of Ru^{II}-OH_2 and Ru^{III}-OH_2 species. A selected set of popular density functionals are employed as the available experimental data presents an opportunity to assess the performance of different level of theories. The computed absolute values are tabulated in the supporting information for all five complexes ($[Ru(trpy)(bpy)(H_2O)]^{2+}$, *trans*-**2**, *cis*-**2**, *trans*-**3** and *cis*-**3** (Tables S4 and S5) but here the discussion will be limited to mean unsigned errors (MUEs) (Table 2). The computed MUEs for redox potentials indicate larger errors for local functionals (M06-L, MN15-L) whereas the hybrid functionals exhibit improved agreement with the experimental results. Ru^{V}-O/Ru^{IV}-O couple is especially important as it requires the highest energy input thus determines the overpotential for WOCs and MN15 and wB97X-D functionals provide excellent agreement with experimental results (Table 2a). An interesting observation is that the only PCET step of the mechanism at pH 1, Ru^{III}-OH_2 to Ru^{IV}-O oxidation, displays the highest MUEs for MN15-L and MN15 functionals. For MN15 functional, this could partly be attributed to free energy changes associated with deprotonation steps as pK_a computations indicate large MUEs compared to best performing functionals M06-L and M06 (Table 2a). Overall, the assessment indicates that tandem of M06 and MN15 functionals could provide a reliable approach for theoretical studies of Ru based WOCs.

Table 2. a) Computed mean unsigned errors (MUEs) of selected set of density functionals for redox potentials of II/III (Ru^{II}-OH_2/ Ru^{III}-OH_2), III/IV (Ru^{III}-OH_2/ Ru^{IV}-O) and IV/V (Ru^{IV}-O/ Ru^{V}-O) couples at pH 1.0 (see Table S4 for the computed absolute values of $[Ru(trpy)(bpy)(H_2O)]^{2+}$, *trans*-**2**, *cis*-**2**, *trans*-**3** and *cis*-**3** complexes). b) Computed mean unsigned errors (MUEs) of selected set of density functionals for pK_as of II (Ru^{II}-OH_2) and III (Ru^{III}-OH_2) (see Table S5 for the computed absolute values of $[Ru(trpy)(bpy)(H_2O)]^{2+}$, *trans*-**2**, *cis*-**2**, *trans*-**3** and *cis*-**3** complexes).

a)

Functional	II/III	III/IV	IV/V	Overall
M06-L	0.37	0.38	0.41	0.39
MN15-L-	0.22	0.67	0.37	0.41
B3LYP-D3	0.32	0.12	0.15	0.21
ωB97X-D	0.37	0.04	0.04	0.16
M06	0.31	0.21	0.13	0.21
MN15	0.11	0.47	0.06	0.19

b)

Functional	II/III	III/IV	Overall
M06-L	1.0	1.1	1.0
MN15-L-	1.3	2.9	2.1
B3LYP-D3	2.4	0.7	1.6
ωB97X-D	4.6	1.2	2.9
M06	0.8	1.3	1.1
MN15	1.4	2.0	1.7

3. 3 Water Oxidation Catalysis: Performance and Mechanism

The kinetics of the water oxidation catalysis by the Ru-aquo complexes in Chart 1 were assessed electrochemically, by using the "foot of the wave analysis" (FOWA), which allows us to calculate the apparent kinetic constant (k_{obs}) from cyclic voltammetry experiments.[65,66,67] This method uses the relationship in equation 8 for a first order kinetics,

$$\frac{i}{i_p} = \frac{4*2.24*\sqrt{\frac{RTk_{obs}}{Fv}}}{1+\exp\left(\frac{F\left(E^0_{P/Q}-E\right)}{RT}\right)} \qquad (8)$$

where i is the current intensity in the presence of substrate, i_p is the current intensity in the absence of substrate (we approximate this current to the current associated with the $Ru^{III/II}$ couple), $E^0_{P/Q}$ is the standard potential for the redox couple that starts the catalysis (1.62 V for *trans*-**2**, 1.71 V for *cis*-**2**, 1.60 V *trans*-**3** and 1.67 for *cis*-**3** extracted from the DPVs in Figure S15), F is the faraday constant, v is the scan rate, and R is 8.314 J mol^{-1} K^{-1}. TOF_{max} or k_{obs} can be extracted from the plot of i/i_p versus 1/{1 + exp[(F/RT)($E_{P/Q}$ − E)]} as shown in Figure S19.

From these calculations, TOF_{max} values of 4.20 s^{-1} for *trans*-**2**, 6.88 s^{-1} for *cis*-**2**, 1.16 s^{-1} for *trans*-**3** and 0.28 s^{-1} for *cis*-**3** were obtained. A plot of TOF_{max} vs. $E_{1/2}(Ru^{V/IV})$ (Figure 5b) graphically shows the existence of a linear correlation, except for complex *cis*-**3,** suggesting that in these complexes the last electron transfer is involved in the rate determining step.[68]

The water oxidation to dioxygen catalytic properties of complexes *trans*-**2**, *trans*-**3** and *cis*-**3** were also tested using a sacrificial oxidant, *i.e.,* $(NH_4)_2[Ce(NO_3)_6]$. Compound *cis*-**2** could not be analyzed due to the limitations of its synthesis that afforded very low yields (see experimental details). The observed catalytic rates follow exactly the same trend as observed in the electrocatalysis, that is, TOF_i (*trans*-**2**) > TOF_i (*trans*-**3**) > TOF_i (*cis*-**3**) (Figure 5a and Table 1). Although *trans*-**2** is the fastest with TOF_i of 0.68 s^{-1} it is less robust than *trans*-**3** with a TOF_i of 0.24 s^{-1} (TON = 14.90, 60% efficiency and TON = 19.87, 80% efficiency, respectively). Complex *cis*-**3** produces 8.4 TON (42% efficiency) with a TOF_i of 0.11 s^{-1} under the same conditions. All catalysts reported here show higher TOF_i than the related complex $[Ru(trpy)(bpy)(H_2O)]^{2+}$ highlighting the role of the carboxylate group in qc and pic ligands (compare entry 1 with entries 3-5 in Table 1). It is important to remark that no time lag of the gas evolution profile was observed (Figure 5a, inset), ruling out any chemical transformation of the catalyst prior to catalysis, a phenomenon that has been proposed for $[Ru(trpy)(bpy)(H_2O)]^{2+}$ under similar catalytic conditions.[69,70] Indeed, cyclic

voltammetry analysis of *trans*-**2** after the catalytic test proves the integrity of the molecular structure of the complex (Figure S23, supporting information).

As summarized in Table 1, the TOF_{max} and TOF_i values of *trans*-**2** and *cis*-**2** are the highest of the family of six coordinated ruthenium-aquo complexes containing a single carboxylate coordinated to the metal center in its active form, including reported complexes $[Ru(pdc)(bpy)(H_2O)]^+$ (pdc = 2,6-pyridinedicarboxylate) and $[Ru(bpc)(bpy)(H_2O)]^+$ (entries 6 and 7).[63,64]

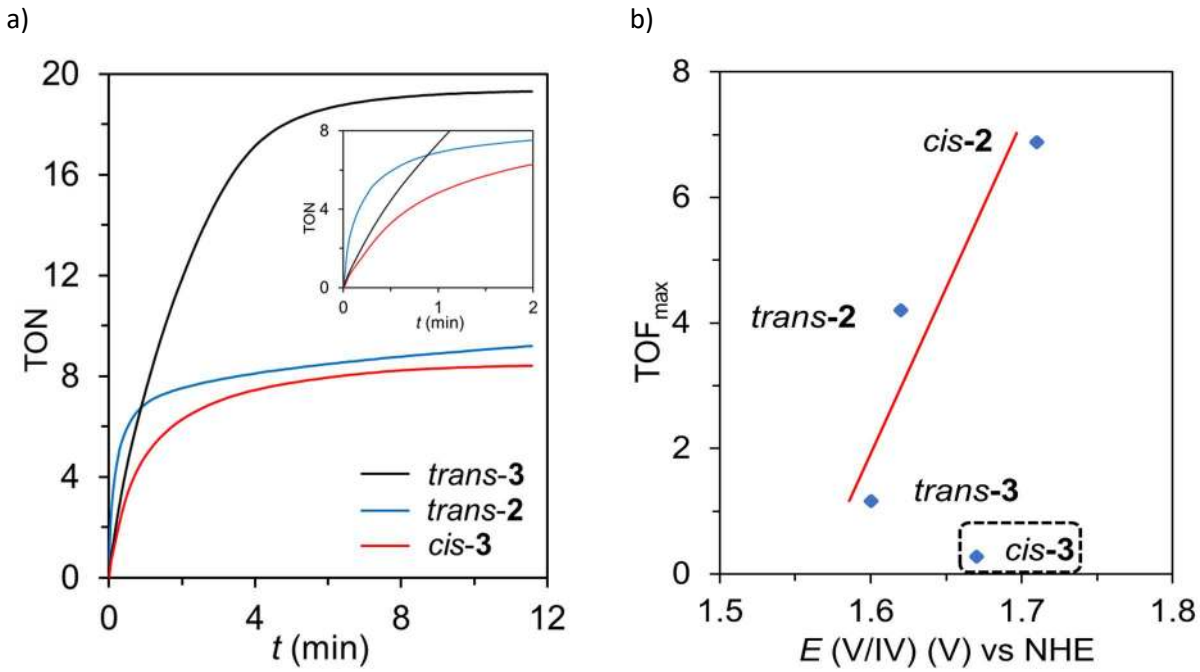

Figure 5. a) Oxygen evolution profile obtained for *trans*-**2** (blue), *trans*-**3** (black) and *cis*-**3** (red). Experimental conditions: 1 mM of complex and 100 mM of Ce^{IV} in 0.1 M triflic acid (2 mL total volume) at 25 ˚C. TON = 25. Inset: same profile for first 2 min. b) Plot of TOF_{max} *vs.* E^o ($Ru^{V/IV}$) for all four complexes obtained from FOWA.

We further performed DFT calculations at M06 and MN15 level of theories to probe the water oxidation mechanisms of *cis*-**2** and *trans*-**2**. A summary of the proposed mechanism of *cis*-**2** at MN15 level of theory is presented in Scheme 2 and further details are available in Scheme S1 and Table S3. At pH 1.0, the activation of the catalyst starts with 1 e^- oxidation of $[Ru^{II}\text{-}OH_2]^+$ to $[Ru^{III}\text{-}OH_2]^{2+}$ (E = 0.69 V) followed by another 1 e^- oxidation with concomitant removal of 2 H^+ to generate $[Ru^{IV}\text{-}O]^+$ (E = 1.23 V). Further 1 e^- oxidation generates the reactive $[Ru^{V}\text{-}O]^{2+}$ species (E = 1.69 V) which performs O-O bond formation via water nucleophilic attack (WNA) pathway ($\Delta G^{\ddagger}$ = 21.7 and ΔG = 0.8 kcal/mol). Since the carboxylate group

is coordinated to the Ru center, it does not facilitate the O-O bond formation to a significant extent in contrast to those seven-coordinated catalysts with pendant carboxylate groups.[6] The resulting $[Ru^{III}\text{-}OOH]^+$ undergoes a PCET step to generate $[Ru^{IV}\text{-}OO]^+$ (E = 1.04 V) which will evolve molecular O_2 and regenerate the initial $[Ru^{II}\text{-}OH_2]^+$ complex ($\Delta G = -8.1$ kcal/mol).

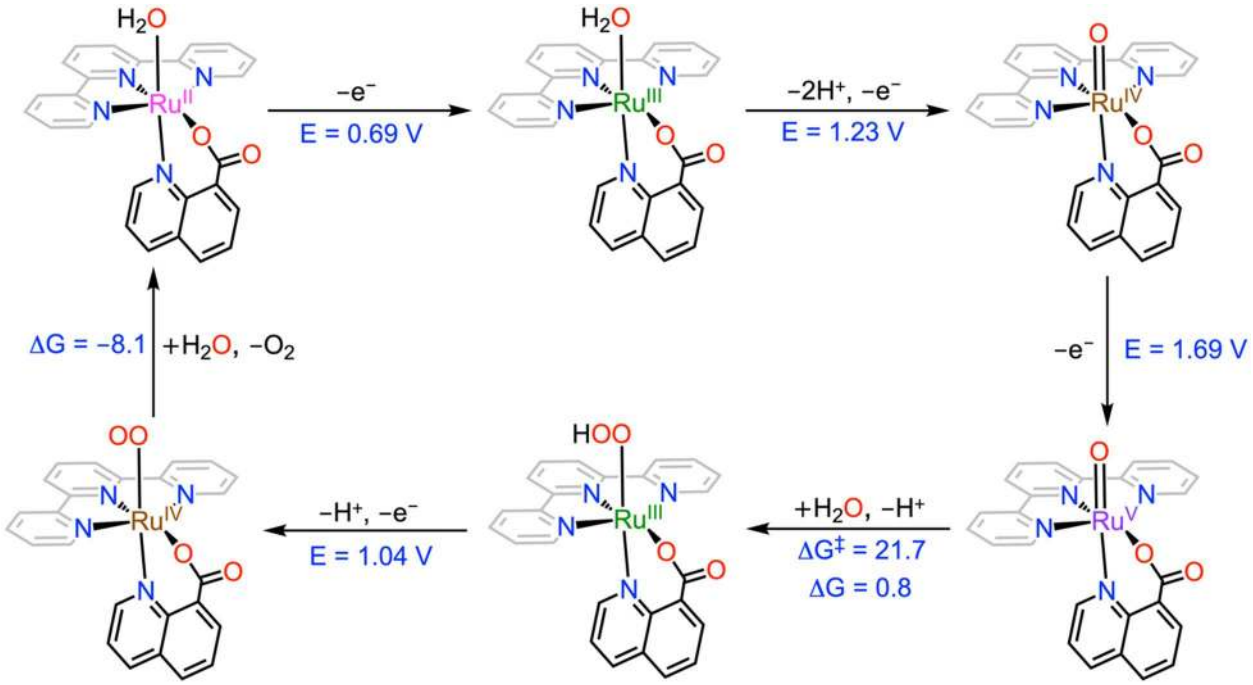

Scheme 2. Proposed water oxidation mechanism of *cis*-**2** at pH 1.0. Computed redox potentials (in units of volts) and free energy changes (in units of kcal/mol) at MN15 level of theory are presented.[71,72]

4. Conclusion

In summary, we have synthesized and characterized a series of ruthenium complexes with bidentate ligands containing carboxylate groups with different isomeric forms. In all the complexes, *trans*-isomers show lower potential of their redox couple as compared to *cis*-isomers due to the different extend of *trans* influence of the carboxylate group in the quinolinato or picolinato ligands. Complexes *cis*-**2** and *trans*-**2** with 6-member chelate ring around the ruthenium turn out to be faster water oxidation catalysts as compare to *cis*-**3** and *trans*-**3** (5-member chelate ring around the ruthenium) with TOF_{max} values of 4.2 s^{-1} for *trans*-**2** and 6.8 s^{-1} for *cis*-**2**. They also outperform other reported ruthenium-aquo complexes $[Ru(pdc)(bpy)(H_2O)]^+$ and $[Ru(bpc)(bpy)(H_2O)]^+$ containing a single carboxylate group.

While previous reports have thoroughly studied the influence of carboxylate groups versus neutral ligands in the water oxidation catalytic activity of Ru complexes, here we go a step forward and evaluate the effects of ligand based geometrical isomerism in Ru complexes. We have analyzed these isomers based on thermodynamic grounds showing how the trans influence affects their redox potentials, and how this in turns is responsible for their catalytic performance.

5. Acknowledgements

M. A. Hoque thanks to "AGAUR" foundation for PhD grant (Ref: 2016 FI_B 01011). The authors gratefully acknowledge the support from Ministerio de Ciencia, Innovacion y Universidades and FEDER (PID2019-111617RB-I00), AGAUR 2017-SGR-1631, Ministerio de Ciencia e Innovacion for a Severo Ochoa Excellence Accreditation grant 2020-2023 (CEX2019-000925-S, MIC/AEI)". GKL acknowledges SERB (New Delhi, India) for financial assistance and J. C. Bose Fellowship. The work at BNL (M.Z.E.) was supported by the U.S. Department of Energy (DOE), Office of Science, Office of Basic Energy Sciences, Division of Chemical Sciences, Geosciences & Biosciences, under Contract No. DE-SC0012704.

6. Supporting Information. Additional experimental details, electrochemical, spectroscopic and computational data. CIF files for complexes *cis*-**1,** *trans*-**1**, *trans*-**2**, and *cis*-[Ru(trpy)(pic)Cl] with CCDC numbers 2055520-2055523 are available at https://www. ccdc.cam.ac.uk/.

7. References

[1] Lewis, N. S. Research opportunities to advance solar energy utilization. Science (Washington, DC, U. S.) **2016**, *351* (6271), No. aad1920.

[2] Berardi, S.; Drouet, S.; Francas, L.; Gimbert-Surinach, C.; Guttentag, M.; Richmond, C.; Stoll, T.; Llobet, A. Molecular artificial photosynthesis. *Chem. Soc. Rev.* **2014**, *43*, 7501.

[3] Sala, X.; Maji, S.; Bofill, R.; Garcia-Anton, J.; Escriche, L. S.; Llobet, A. Molecular water oxidation mechanisms followed by transition metals: State of the art. *Acc. Chem. Res.* **2013**, *47*, 504.

[4] Gersten, S. W.; Samuels, G. J.; Meyer, T. J. Catalytic oxidation of water by an oxo-bridged ruthenium dimer. *J. Am. Chem. Soc.* **1982**, *104*, 4029.

[5] Duan, L.; Bozoglian, F.; Mandal, S.; Stewart, B.; Privalov, T.; Llobet, A.; Sun, L. A molecular ruthenium catalyst with water-oxidation activity comparable to that of photosystem II. *Nat. Chem.* **2012**, *4*, 418.

[6] Matheu, R.; Ertem, M. Z.; Benet-Buchholz, J.; Coronado, E.; Batista, V. S.; Sala, X.; Llobet, A. Intramolecular proton transfer boosts water oxidation catalyzed by a Ru complex. *J. Am. Chem. Soc.* **2015**, *137*, 10786.

[7] Hoque, M. A.; Benet-Buchholz, J.; Llobet, A.; Gimbert-Suriñach, C. Catalytic oxidation of water to dioxygen by mononuclear Ru complexes bearing a 2, 6-Pyridinedicarboxylato ligand. *ChemSusChem* **2019**, *12*, 1949.

[8] Shatskiy, A.; Bardin, A. A.; Oschmann, M.; Matheu, R.; Benet-Buchholz, J.; Eriksson, L.; Kärkäs, M. D.; Johnston, E. V.; Gimbert-Suriñach, C.; Llobet, A.; Åkermark, B. Electrochemically driven water oxidation by a highly active ruthenium-based catalyst. *ChemSusChem* **2019**, *12*, 2251.

[9] Vereshchuk, N.; Matheu, R.; Benet-Buchholz, J.; Pipelier, M.; Lebreton, J.; Dubreuil, D.; Tessier, A.; Gimbert-Suriñach, C.; Ertem, M. Z.; Llobet, A. Second coordination sphere effects in an evolved Ru complex based on a highly adaptable ligand results in rapid water oxidation catalysis. *J. Am. Chem. Soc.* **2020**, *142*, 5068.

[10] Wang, L.; Duan, L.; Tong, L.; Sun, L. Visible light-driven water oxidation catalyzed by mononuclear ruthenium complexes. *J. Catal.* **2013**, *306*, 129.

[11] Roeser, S.; Farràs, P.; Bozoglian, F.; Martínez-Belmonte, M.; Benet-Buchholz, J.; Llobet, A. Chemical, electrochemical, and photochemical catalytic oxidation of water to dioxygen with mononuclear ruthenium complexes. *ChemSusChem* **2011**, *4*, 197.

[12] Berardi, S.; Francàs, L.; Neudeck, S.; Maji, S.; Benet-Buchholz, J.; Meyer, F.; Llobet, A. Efficient light-driven water oxidation catalysis by dinuclear ruthenium complexes. *ChemSusChem.* **2015**, *8*, 3688.

[13] Li, H.; Li, F.; Zhang, B.; Zhou, X.; Yu, F.; Sun, L. Visible light-driven water oxidation promoted by host–guest interaction between photosensitizer and catalyst with a high quantum efficiency. *J. Am. Chem. Soc.* **2015**, *137*, 4332.

[14] Francàs, L.; Matheu, R.; Pastor, E.; Reynal, A.; Berardi, S.; Sala, X.; Llobet, A.; Durrant, J. R. Kinetic analysis of an efficient molecular light-driven water oxidation system. *ACS Catal.* **2017**, *7*, 5142.

[15] Concepcion, J. J.; Tsai, M.-K.; Muckerman, J. T.; Meyer, T. J. Mechanism of water oxidation by single-site ruthenium complex catalysts. *J. Am. Chem. Soc.* **2010**, *132*, 1545

[16] Vigara, L.; Ertem, M. Z.; Planas, N.; Bozoglian, F.; Leidel, N.; Dau, H.; Haumann, M.; Gagliardi, L.; Cramer, C. J.; Llobet, A. Experimental and quantum chemical characterization of the water oxidation cycle catalysed by $[Ru^{II}(damp)(bpy)(H_2O)]^{2+}$. *Chem. Sci.* **2012**, *3*, 2576.

[17] Pushkar, Y.; Moonshiram, D.; Purohit, V.; Yan, L.; Alperovich, I. Spectroscopic analysis of catalytic water oxidation by $[Ru^{II}(bpy)(tpy)H_2O]^{2+}$ suggests That Ru^{V}=O is not a rate-limiting intermediate. *J. Am. Chem. Soc*. **2014**, *136*, 11938.

[18] Pushkar, Y.; Pineda-Galvan, Y.; Ravari, A. K.; Otroshchenko, T.; Hartzler, D. A. Mechanism for O–O bond formation via radical coupling of metal and ligand based radicals: A new pathway. *J. Am. Chem. Soc.* **2018**, *140*, 13538.

[19] Moonshiram, D.; Pineda-Galvan, Y.; Erdman, D.; Palenik, M.; Zong, R.; Thummel, R.; Pushkar, Y. Uncovering the Role of Oxygen Atom Transfer in Ru-Based Catalytic Water Oxidation. *J. Am. Chem. Soc*. **2016**, *138*, 15605.

[20] Ertem, M. Z, Concepcion, J. J.: Oxygen atom transfer as an alternative pathway for oxygen-oxygen bond formation, *Inorg. Chem.,* **2020**, *59*, 5966.

[21] Barnett, S. M.; Goldberg, K. I.; Mayer, J. M. A soluble copper–bipyridine water-oxidation electrocatalyst. *Nat. Chem.* **2012**, *4*, 498.

[22] Sens, C.; Romero, I.; Rodríguez, M.; Llobet, A.; Parella, T.; Benet-Buchholz, J. A new Ru complex capable of catalytically oxidizing water to molecular dioxygen. *J. Am. Chem. Soc.* **2004**, *126*, 7798.

[23] Neudeck, S.; Maji, S.; López, I.; Meyer, S.; Meyer, F.; Llobet, A. New powerful and oxidatively rugged dinuclear Ru water oxidation catalyst: Control of mechanistic pathways by tailored ligand design. *J. Am. Chem. Soc.* **2013**, *136*, 24.

[24] Schulze, M.; Kunz, V.; Frischmann, P. D.; Würthner, F. A supramolecular ruthenium macrocycle with high catalytic activity for water oxidation that mechanistically mimics photosystem II. *Nat. Chem.* **2016**, *8*, 576.

[25] Gimbert-Suriñach, C.; Moonshiram, D.; Francàs, L.; Planas, N.; Bernales, V.; Bozoglian, F.; Guda, A.; Mognon, L.; López, I.; Hoque, M. A.; Gagliardi, L.; Cramer, C. J.; Llobet, A. Structural and spectroscopic characterization of reaction intermediates involved in a dinuclear Co–hbpp water oxidation catalyst. *J. Am. Chem. Soc.* **2016**, *138*, 15291

[26] Sullivan, B. P.; Calvert, J. M.; Meyer, T. J. Cis-trans isomerism in (trpy)(PPh_3) $RuCl_2$. Comparisons between the chemical and physical properties of a cis-trans isomeric pair. *Inorg. Chem.* **1980**, *19*, 1404.

[27] Llobet, A.; Doppelt, P.; Meyer, T. J. Redox properties of aqua complexes of ruthenium (II) containing the tridentate ligands 2, 2': 6', 2"-terpyridine and tris (1-pyrazolyl) methane. *Inorg. Chem.* **1988**, *27*, 514.

[28] Data collection with APEX II version v2013.4-1. Bruker (**2007**). Bruker AXS Inc., Madison, Wisconsin, USA.

[29] Data reduction with Bruker SAINT version V8.30c. Bruker (**2007**). Bruker AXS Inc., Madison, Wisconsin, USA.

[30] Blessing, R. An Empirical Correction for Absorption Anisotropy. *Acta Crysta. A* **1995**, *51*, 33.

[31] Data collection and reduction with CrysAlisPro 1.171.39.12b (Rigaku OD, **2015**).

[32] Empirical absorption corrrection using spherical harmonics implemented in Scale3 Abspack scaling algorithm, CrysAlisPro 1.171.39.12b (Rigaku OD, **2015**).

[33] Sheldrick, G. Shelxt - Integrated Space-Group and Crystal-Structure Determination. *Acta Crysta. A* **2015**, *71*, 3.

[34] Hubschle, C. B.; Sheldrick, G. M.; Dittrich, B. Shelxle: A Qt Graphical User Interface for Shelxl. *J. Appl. Crystallogr.* **2011**, *44*, 1281-1284.

[35] Sheldrick, G. Crystal Structure Refinement with Shelxl. *Acta Cryst. C* **2015**, *71*, 3.

[36] Zhao, Y.; Truhlar, D. G. The M06 suite of density functionals for main group thermochemistry, thermochemical kinetics, noncovalent interactions, excited states, and transition elements: two new functionals and systematic testing of four M06-class functionals and 12 other functionals.*Theor. Chem. Acc.* **2008**, *120*, 215–241.

[37] Marenich, A. V.; Cramer, C. J.; Truhlar, D. G. Universal solvation model based on solute electron density and on a continuum model of the solvent defined by the bulk dielectric constant and atomic surface tensions. *J. Phys. Chem. B* **2009**, *113*, 6378-6396.

[38] Andrae, D.; Häußermann, U.; Dolg, M.; Stoll, H.; Preuß, H. Energy-adjustedab initio pseudopotentials for the second and third row transition elements. *Theor. Chim. Acta.* **1990** *77*, 123-141.

[39] Hehre, W. J. *Ab Initio Molecular Orbital Theory*; Wiley, 1986.

[40] Gaussian 16, Revision C.01, Frisch, M. J.; Trucks, G. W.; Schlegel, H. B.; Scuseria, G. E.; Robb, M. A.; Cheeseman, J. R.; Scalmani, G.; Barone, V.; Petersson, G. A.; Nakatsuji, H.; Li, X.; Caricato, M.; Marenich, A. V.; Bloino, J.; Janesko, B. G.; Gomperts, R.; Mennucci, B.; Hratchian, H. P.; Ortiz, J. V.; Izmaylov, A. F.; Sonnenberg, J. L.; Williams-Young, D.; Ding, F.; Lipparini, F.; Egidi, F.; Goings, J.; Peng, B.; Petrone, A.; Henderson, T.; Ranasinghe, D.; Zakrzewski, V. G.; Gao, J.; Rega, N.; Zheng, G.; Liang, W.; Hada, M.; Ehara, M.; Toyota, K.; Fukuda, R.; Hasegawa, J.; Ishida, M.; Nakajima, T.; Honda, Y.; Kitao, O.; Nakai, H.; Vreven, T.; Throssell, K.; Montgomery, J. A., Jr.; Peralta, J. E.; Ogliaro, F.; Bearpark, M. J.; Heyd, J. J.; Brothers, E. N.; Kudin, K. N.; Staroverov, V. N.; Keith, T. A.; Kobayashi, R.; Normand, J.; Raghavachari, K.; Rendell, A. P.; Burant, J. C.; Iyengar, S. S.; Tomasi, J.; Cossi, M.; Millam, J. M.; Klene, M.; Adamo, C.; Cammi, R.; Ochterski, J. W.; Martin, R. L.; Morokuma, K.; Farkas, O.; Foresman, J. B.; Fox, D. J. Gaussian, In., Wallingford CT, **2016**.

[41] Cramer, C. J. *Essentials of Computational Chemistry: Theories and Models*; Wiley, **2013**.

[42] Zhao, Y.; Truhlar, D. G., A new local density functional for main-group thermochemistry, transition metal bonding, thermochemical kinetics, and noncovalent interactions. *J. Chem. Phys.* **2006,** *125*, 194101.

[43] Yu, H. S., He, X., Truhlar, D. G. MN15-L: A new local exchange-correlation functional for Kohn–Sham density functional theory with broad accuracy for atoms, molecules, and solids, *J. Chem. Theory Comput.* **2016**, *12*, 1280.

[44] Becke, A. D. A definitive example of aluminum-27 chemical shielding anisotropy. *J. Chem. Phys*. **1993**, *98*, 5648.

[45] S. Grimme, S. Ehrlich and L. Goerigk, Effect of the damping function in dispersion corrected density functional theory. *J. Comp. Chem.* **2011,** *32,* 1456.

[46] Chai, J. D.; Head-Gordon, M., Long-range corrected hybrid density functionals with damped atom–atom dispersion corrections. *Phys. Chem. Chem. Phys*. **2008**, *10*, 6615.

[47] Yu, H. S., He, X., Li, S. L., Truhlar, D. G. MN15: A Kohn-Sham Global-Hybrid exchange-correlation density functional with broad accuracy for multi-reference and single-reference systems and noncovalent interactions. *Chem. Sci.* **2016**, *7*, 5032.

[48] Tissandier, M. D.; Cowen, K. A.; Feng, W. Y.; Gundlach, E.; Cohen, M. H.; Earhart, A. D.; Coe, J. V.; Tuttle, T. R. The proton's absolute aqueous enthalpy and Gibbs free energy of solvation from cluster-ion solvation data. *J. Phys. Chem. A* **1998**, *102*, 7787.

[49] Camaioni, D. M.; Schwerdtfeger, C. A. Comment on "Accurate Experimental Values for the Free Energies of Hydration of H^+, OH^-, and $H3O^{+}$". *J. Phys. Chem. A* **2005**, *109*, 10795.

[50] Kelly, C. P.; Cramer, C. J.; Truhlar, D. G. Aqueous solvation free energies of ions and ion− water clusters based on an accurate value for the absolute aqueous solvation free energy of the proton. *J. Phys. Chem. B* **2006**, *110*, 16066.

[51] Bryantsev, V. S.; Diallo, M. S.; Goddard, W. A. Calculation of solvation free energies of charged solutes using mixed cluster/continuum models. *J. Phys. Chem. B* **2008**, *112*, 9709.

[52] Lewis, A.; Bumpus, J. A.; Truhlar, D. G.; Cramer, C. J. Molecular modeling of environmentally important processes: Reduction potentials. *J. Chem. Ed.* **2004**, *81*, 596.

[53] Winget, P.; Cramer, C. J.; Truhlar, D. G. Computation of equilibrium oxidation and reduction potentials for reversible and dissociative electron-transfer reactions in solution. *Theor. Chem. Acc.* **2004**, *112*, 217-227.

[54] Mandal, A.; Hoque, M. A.; Grupp, A.; Paretzki, A.; Kaim, W.; Lahiri, G. K. Analysis of redox series of unsymmetrical 1, 4-diamido-9, 10-anthraquinone-bridged diruthenium compounds. *Inorg. Chem.* **2016**, *55*, 2146.

[55] Maji, S.; López, I.; Bozoglian, F.; Benet-Buchholz, J.; Llobet, A. Mononuclear ruthenium–water oxidation catalysts: discerning between electronic and hydrogen-bonding effects. *Inorg. Chem.* **2013**, *52*, 3591.

[56] Chanda, N.; Mobin, S. M.; Puranik, V. G.; Datta, A.; Niemeyer, M.; Lahiri, G. K. Stepwise synthesis of $[Ru(trpy)(L)(X)]^{n+}$ (trpy = 2,2′:6′,2′ ′-Terpyridine; L = 2,2′-Dipyridylamine; X = Cl^-, H_2O, NO_2^-, NO^+, O_2^-). Crystal structure, spectral, electron-transfer, and photophysical aspects. *Inorg. Chem.* **2004**, *43*, 1056.

[57] Mondal, B.; Paul, H.; Puranik, V. G.; Lahiri, G. K. Ruthenium terpyridine complexes incorporating azo-imine based ancillary ligands. Synthesis, crystal structure, spectroelectrochemical properties and solution reactivities. *J. Chem. Soc., Dalton Trans.* **2001**, 4209

[58] Patra, S.; Sarkar, B.; Ghumaan, S.; Patil, M. P.; Mobin, S. M.; Sunoj, R. B.; Kaim, W.; Lahiri, G. K. Isomeric ruthenium terpyridine complexes $[Ru(trpy)(L)Cl]^{n+}$ containing the unsymmetrically bidentate acceptor L = 3-amino-6-(3,5-dimethylpyrazol-1-yl)-1,2,4,5-tetrazine. Synthesis, structures, electrochemistry, spectroscopy and DFT calculations. *Dalton. Trans.* **2005**, 1188.

[59] Chowdhury, A. D.; Das, A.; Mobin, S. M.; Lahiri, G. K. Isomeric complexes of $[Ru^{II}(trpy)(L)Cl]$ (trpy = 2,2′:6′,2′′-Terpyridine and HL = Quinaldic Acid): Preference of isomeric structural form in catalytic chemoselective epoxidation process. *Inorg. Chem.* **2011**, *50*, 1775.

[60] Mognon, L.; Benet-Buchholz, J.; Rahaman, S. W.; Bo, C.; Llobet, A. Ru–Zn heteropolynuclear complexes containing a dinucleating bridging ligand: Synthesis, structure, and isomerism. *Inorg. Chem.* **2014**, *53*, 12407

[61] Mognon, L.; Benet-Buchholz, J.; Llobet, A. Single site isomeric Ru wocs with an electron-withdrawing group: synthesis, electrochemical characterization, and reactivity. *Inorg. Chem.* **2015**, *54*, 11948.

[62] Takeuchi, K. J.; Thompson, M. S.; Pipes, D. W.; Meyer, T. J. Redox and spectral properties of monooxo polypyridyl complexes of ruthenium and osmium in aqueous media. *Inorg. Chem.* **1984**, *23*, 1845.

[63] Hoque, M. A.; Gil-Sepulcre, M.; Benet-Buchholz, J.; Llobet, A.; Gimbert-Suriñach, C. Synthesis, electrochemical characterization and water oxidation chemistry of Ru complexes containing the 2,6-pyridinedicarboxylato ligand. *Inorg. Chem.* **2020,** *59*, 11432.

[64] Tong, L.; Inge, A. K.; Duan, L.; Wang, L.; Zou, X.; Sun, L. Catalytic water oxidation by mononuclear Ru complexes with an anionic ancillary ligand. *Inorg. Chem.* **2013**, *52*, 2505.

[65] Costentin, C.; Drouet, S.; Robert, M.; Savéant, J.-M. A local proton source enhances CO_2 electroreduction to CO by a molecular Fe catalyst. *Science* **2012**, *338*, 90.

[66] Costentin, C.; Drouet, S.; Robert, M.; Savéant, J.-M. Turnover numbers, turnover frequencies, and overpotential in molecular catalysis of electrochemical reactions. Cyclic voltammetry and preparative-scale electrolysis. *J. Am. Chem. Soc.* **2012**, *134*, 11235

[67] Matheu, R.; Neudeck, S.; Meyer, F.; Sala, X.; Llobet, A. Foot of the wave analysis for mechanistic elucidation and benchmarking applications in molecular water oxidation catalysis. *ChemSusChem* **2016**, *9*, 3361.

[68] Marcus Theory: Thermodynamics CAN Control the Kinetics of Electron Transfer Reactions. Silverstein, T. P. *J. Chem. Educ.* **2012**, *89*, 1159.

[69] Ravari, A. K.; Zhu, G.; Ezhov, R.; Pineda-Galvan, Y.; Page, A.; Weinschenk, W.; Yan, L.; Pushkar, Y. Unraveling the mechanism of catalytic water oxidation via de novo synthesis of reactive intermediate. *J. Am. Chem. Soc.* **2020**, *142*, 884.

[70] López, I.; Ertem, M. Z.; Maji, S.; Benet-Buchholz, J.; Keidel, A.; Kuhlmann, U.; Hildebrandt, P.; Cramer, C. J.; Batista, V. S.; Llobet, A. *Angew. Chem. Int. Ed.* **2014**, *53*, 205.

[71] Wasylenko, D. J.; Ganesamoorthy, C.; Henderson, M. A.; Koivisto, B. D.; Osthoff, H. D.; Berlinguette, C. P. Electronic modification of the $[Ru^{II}(tpy)(bpy)(OH_2)]^{2+}$ scaffold: Effects on catalytic water oxidation. *J. Am. Chem. Soc*. **2010**, *132*, 16094.

[72] Matheu, R.; Ertem, M. Z.; Gimbert-Suriñach, C.; BenetBuchholz, J.; Sala, X.; Llobet, A. Hydrogen bonding rescues overpotential in seven-coordinated Ru water oxidation catalysts. *ACS Catal.* **2017**, **7**, 6525.

TOC

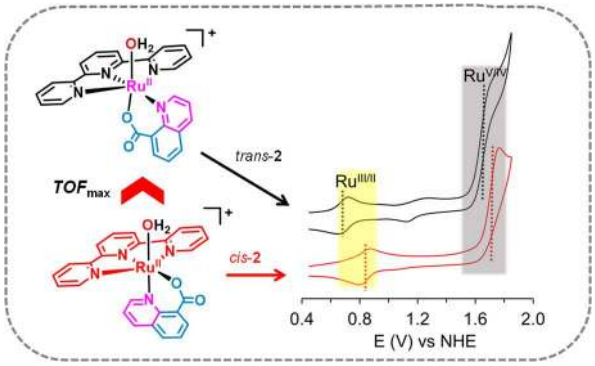
OH2
Ru^II
trans-2
TOF_max
cis-2
Ru^III/II
Ru^V/IV
0.4
0.8
1.2
1.6
2.0
E (V) vs NHE